Applied Acoustics 152 (2019) 31–40

Contents lists available at ScienceDirect

Applied Acoustics

journal homepage: www.elsevier.com/locate/apacoust

On the low frequency acoustic properties of novel multifunctional honeycomb sandwich panels with micro-perforated faceplates

H. Meng [a,b,c], M.A. Galland [b,*], M. Ichchou [c,*], F.X. Xin [a], T.J. Lu [a]

[a] MOE Key Laboratory for Multifunctional Materials and Structures, Xi'an Jiaotong University, Xi'an 710049, PR China
[b] Univ Lyon, École Centrale de Lyon, Laboratoire de Mécanique des Fluides et d'Acoustique, UMR CNRS 5509, F-69134 Écully, France
[c] Laboratoire de Tribologie et Dynamique des Systèmes, École Centrale de Lyon, 36, Avenue Guy de Collongues, 69130 Ecully Cedex, France

ARTICLE INFO

Article history:
Received 31 October 2018
Received in revised form 24 February 2019
Accepted 26 February 2019
Available online 27 March 2019

Keywords:
Sandwich structures
Honeycomb
Microperforated
Multifunctional
Sound absorption
Sound transmission loss

ABSTRACT

This paper explores further possibilities of structurally-efficient honeycomb sandwich panels by replacing one of the faceplates with the perforated faceplate from the viewpoint of sound absorption coefficient (SAC) as well as sound transmission loss (STL). An analytical model is presented to calculate both the STL and SAC, with the displacements of the two faceplates assumed identical at frequencies below the faceplate resonance frequency. Influences of core configuration are investigated by comparing different honeycomb core designs. Finite element (FE) models are subsequently developed to validate the proposed analytical model, with agreement achieved. Subsequently, parametric surveys, including the influences of perforation ratio, pore size and core configuration on STL and SAC, are conducted based on the analytical model. Unlike classical honeycomb sandwich panels which are poor sound absorbers, honeycomb sandwiches with perforated faceplates lead to high SAC at low frequencies, which in turn brings about increment in the low frequency STL. Moreover, sandwich panels with triangular cores are found to have the lowest peak frequency in the STL and SAC curves compared with the other kinds of sandwich panels having the same effective mass and perforations.

1. Introduction

Sandwich panels are lightweight structures composed of thin faceplates with inserted low density cores. With high stiffness-to-density ratio, good thermal and acoustic properties, sandwich panels have been widely applied in packaging, transportation, aerospace, and building/construction fields. Nonetheless, optimization issues and better understandings of the multi-physical behaviors of sandwich structures remain challenging questions for both academics and industrials.

The concern in what follows is about improving the vibroacoustic properties of sandwich panels. The STL of a sandwich panel, for instance, has attracted numerous investigations. These investigations can be classified by the configuration of core inside the sandwich panel. The simplest sandwich panel is made of double walls with internal air layer. London [1], Antonio et al. [2], Chazot and Guyader [3], and Wang et al. [4] calculated the STL of both infinite and finite sized double walls separated by air gaps using analytical modeling and statistical energy analysis. To improve the sound insulation capacity, porous elastic materials are added to fill the gap between the two walls (faceplates), and the lined porous material can be either bounded or unbounded to the faceplates. Bolton et al. [5,6], Panneton and Atalla [7], Kang and Bolton [8] presented theoretical and numerical investigations for the transmission loss of double panels lined with porous materials, with the latter described using the Biot theory [9,10]. They found that the highest STL can be obtained if the porous material is bounded to one faceplate and separated from the other one. Except from porous elastic materials, Chazot and Guyader [11], Doutres and Atalla [12], and Ghanbari et al. [13] also conducted analytical investigations for acoustic properties of double panels with poro-granular materials, thin film damping and multilayer porous blankets, while Zielinski et al. [14] and Hu et al. [15], Melon et al. [16] numerically investigated the sound insulation and transmission properties of active hybrid sandwich panels with porous absorbent material layers in either active or passive mode. Compared with double panels separated by air, sandwich panels filled with porous sound absorbing materials have better sound insulation. However, due to their intrinsically low stiffness, the low-frequency transmission loss of sandwich panels filled with porous materials is yet sufficient. Therefore, many investigators resorted to sandwich panels cored with solid connecting structures to achieve higher stiffness and

* Corresponding authors.
E-mail addresses: marie-annick.galland@ec-lyon.fr (M.A. Galland), mohamed.ichchou@ec-lyon.fr (M. Ichchou).

https://doi.org/10.1016/j.apacoust.2019.02.028
0003-682X/

better low frequency transmission loss, including sandwich panels with stiffened faceplates, corrugated and honeycomb cores. Shen et al. [17] conducted analytical studies for simply supported finite sandwich panels with corrugated cores by employing an equivalent structure of double panels connected by rotational and translational springs. Sun and Liu [18] analyzed the vibration of composite panels with hard coating. Mead [19], Wang et al. [20], Craik and Smith [21] proposed various theories to investigate the transmission loss of double panels connected by parallel plates. Xin and Lu [22] and Shen et al. [23] extended the theories for double plates reinforced with parallel rib stiffeners to orthogonal rib stiffeners. In comparison, sandwich panels with honeycomb cores are the most popular sandwich constructions in application. In addition to characterizing their structural behavior, many studies have also been carried out to characterize their vibroacoustic behavior. For typical instance, Kumar et al. [24], Jung et al. [25], Huang and Ng [26], and Ng and Hui [27] presented theoretical models to predict the STL of honeycomb sandwiches, while Griese et al. [28] and Feng and Kumar [29] employed numerical and experimental methods to investigate their STL.

Apart from the STL, SAC has also become a noticeable issue for investigators of sandwich panels design. In general, even though efficient in STL, sandwich panels are poor sound absorbers. Instead, micro perforated panels (MPPs) can provide good SAC and hence have been widely applied as sound absorbers. A MPP absorber is comprised of a thin plate with perforated submillimeter pores, an air cavity and a rigid wall. Compared with conventional porous absorbing materials, MPP absorbers can provide sufficient wideband absorption at low frequencies. Based on the method of electro-acoustic analogy, Maa [30,31] developed the most popular theory for MPPs. Atalla and Sgard [32] also presented an analytical model to calculate the SAC of MPPs by making use of the theory for rigid frame porous materials.

MPPs can be made of metal, plastic, plywood, acryl glass and sheet material, thus suitable for many environments including even severe conditions. For example, Asdrubali and Pispola [33] applied transparent MPPs as noise barriers, Li and Mechefske [34] experimentally investigated the application of MPPs in magnetic resonance imaging scanners, Sakagami et al. [35] presented investigations of MPP absorbers as room interior surface.

To obtain lightweight structures with good absorption and insulation properties, combinations of MPPs and sandwich panels come into view of several researchers. Dupont et al. [36] investigated an infinite MPP-solid plate coupling structure, both theoretically and experimentally. Tang et al. [37] created a lightweight rigid-frame sandwich panel with perforated honeycomb-corrugation hybrid core as well as perforated faceplates, which exhibited perfect sound absorption at low frequencies. Bravo et al. [38,39] presented a fully coupled modal method to calculate the STL and SAC of finite flexible MPP coupled with plates. Toyoda and Takahashi [40] inserted subdivisions to the middle layer of a MPP-plate structure, achieving improved STL at mid frequencies. These studies demonstrated that MPP-plate sandwich structures have good STL as well as SAC.

Based on the MPP-plate coupling strategy, a novel multifunctional structure that combines honeycomb sandwich panels with perforated faceplates is developed in the present paper. Honeycomb sandwich panels have great STL (and excellent mechanical properties), and the perforated faceplates can act as sound absorbing structures. Section 2 gives a specific description of the investigated structure. Section 3 presents an analytical model to calculate the STL and SAC, with the influence of core configurations embodied in the analytical model. Finite element (FE) models are subsequently developed for validation in Section 4. Perforated faceplates are shown to improve significantly the STL and SAC of honeycomb sandwich panels at low frequencies by systematic parameter studies presented in Section 5. Results obtained in the present paper can be helpful for the design of multifunctional sandwich panels having excellent mechanical properties and superior acoustic properties at low frequencies.

2. Problems description

Consider an ultra-lightweight sandwich panel with hexagonal honeycomb core shown schematically in Fig. 1. Its faceplates and core are both made of homogeneous and isotropic material. The top faceplate is a micro-perforated plate with submillimeter pores to enable sound penetration into the air cavities for absorption. It should be noted that in the structure, to achieve high structural efficiency, the thickness of either faceplate is much smaller than that of the middle layer (i.e., the core), while the wall thickness of the core is much smaller than its edge length. Except from the hexagonal honeycomb, other honeycombs, such as rectangular or triangular honeycombs shown in Fig. 2 can also act as the core of the sandwich. The sandwich panels with micro-perforated faceplates shown in Figs. 1 and 2 are attractive for multifunctional applications requiring lightweight and simultaneous load carrying, sound insulation as well as sound absorption capabilities.

To calculate the STL and SAC of honeycomb sandwich panels with perforated faceplates, an analytical model is set up in the following section. Different from the existing models for normal honeycomb sandwich panels without perforation, this analytical model can calculate the pressure and velocity distributions inside honeycomb sandwich panels with perforated faceplates. Furthermore, influences of the mass and configurations of honeycomb cores on acoustic properties of perforated sandwich panels, that are generally ignored in existing papers for micro-perforated panels such as Ref. [40], are addressed explicitly in the analytical model.

3. Theory

For a normally incident sound wave, the incident sound pressure $p_i(\mathbf{r},z)$ and velocity $v_i(\mathbf{r},z)$ are given as:

$$p_i(\mathbf{r},z) = P_0 e^{-jk_0 z} \quad v_i(\mathbf{r},z) = P_0 e^{-jk_0 z}/\rho_0 c_0 \tag{1}$$

where $k_0 = \omega/c_0$ is the wave number, ω is the angular frequency, c_0 is the sound speed, ρ_0 is the density of air and P_0 is the amplitude of the incident wave. For simplification, the time factor $e^{j\omega t}$ is suppressed and $P_0 = 1$ is set in the present paper.

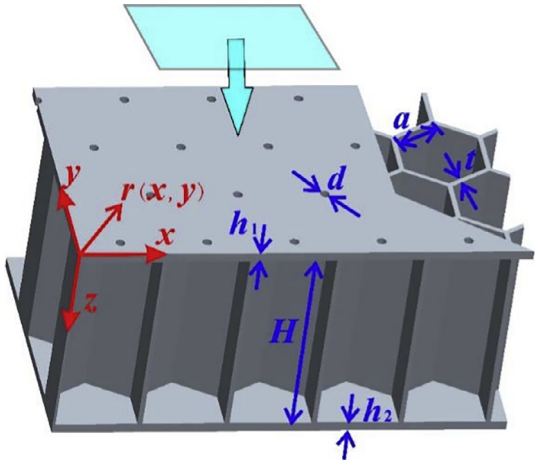

Fig. 1. Schematic of surface-perforated sandwich panel with hexagonal core.

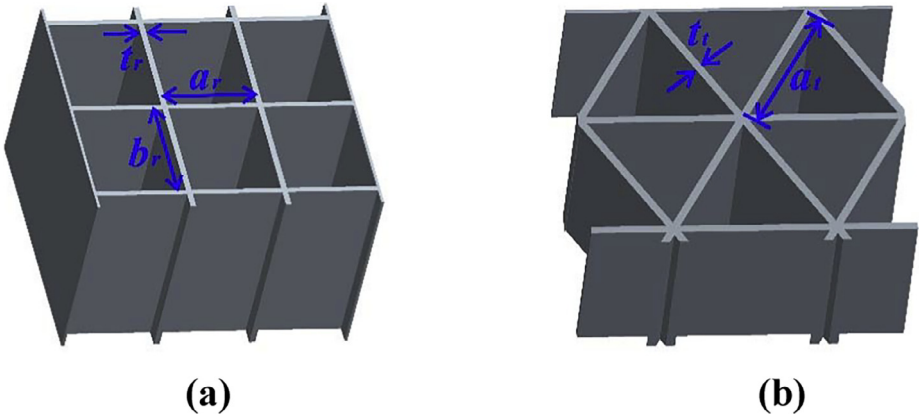

Fig. 2. Top view of sandwich panel with (a) rectangular core and (b) triangular core.

In the field inside the honeycomb core between the faceplates, the sound pressure $p_2(\mathbf{r},z)$ can be given as [40]

$$p_2(\mathbf{r},z) = Ce^{-jk_0(z-h_1)} + De^{jk_0(z-h_1)} \tag{2}$$

where C and D are unknown parameters to be determined, and h_1 is the thickness of the micro-perforated faceplate. Accordingly, the velocity inside the honeycomb can be obtained as:

$$v_2(\mathbf{r},z) = \frac{-1}{j\omega\rho_0}\frac{\partial p_2(\mathbf{r},z)}{\partial z} = \frac{1}{\rho_0 c_0}\left(Ce^{-jk_0(z-h_1)} - De^{jk_0(z-h_1)}\right) \tag{3}$$

According to the Green's function, sound pressures on the surfaces of the faceplates in the incident and transmitted sound fields are separately given by [41]

$$p_1(\mathbf{r}) = 2p_i(\mathbf{r},0) - \frac{\rho_0\omega}{2}\int_{-\infty}^{\infty}\mathbf{H}_0^{(1)}(k_0|\mathbf{r}-\mathbf{r}_0|)v_1(\mathbf{r}_0)d\mathbf{r}_0 \tag{4}$$

$$p_3(\mathbf{r}) = \frac{\rho_0\omega}{2}\int_{-\infty}^{\infty}\mathbf{H}_0^{(1)}(k_0|\mathbf{r}-\mathbf{r}_0|)v_3(\mathbf{r}_0)d\mathbf{r}_0 \tag{5}$$

where $\mathbf{H}_0^{(1)}$ is the first kind Hankel function of zero order. The velocity adjacent to the micro-perforated faceplate is given as [42,43]

$$v_1(\mathbf{r}) = v_2(\mathbf{r},h_1) = (1-\sigma)v_p(\mathbf{r}) + \sigma v_f(\mathbf{r}) \tag{6}$$

where $v_p(\mathbf{r})$ is the velocity of the perforated faceplate, $v_f(\mathbf{r})$ is the velocity of the fluid inside the perforated pores, and σ is the perforation ratio of the plate. For a sandwich panel with hexagonal section core, the perforation ratio is calculated by:

$$\sigma = \pi d^2/6\sqrt{3}a^2 \tag{7}$$

where a is the edge length of the honeycomb, and d is the diameter of the perforated pores as shown in Fig. 1. Likewise, for sandwich panels with rectangular and triangular honeycomb cores, the perforation ratios can be obtained by:

$$\sigma_r = \pi d^2/4a_r b_r \tag{8}$$

$$\sigma_t = \pi d^2/\sqrt{3}a_t^2 \tag{9}$$

where a_r and b_r are the side length of the rectangular honeycomb, and a_t is the edge length of the triangular honeycomb as shown in Fig. 2. The pressure difference between the two surfaces of the perforated faceplate is related to the velocity and impedance, given as:

$$\Delta p(r) = Z_{resist}\left(v_f(\mathbf{r}) - v_p(\mathbf{r})\right) + Z_{react}v_f(\mathbf{r}) \tag{10}$$

where Z_{resist} and Z_{react} are the resistance and reactance of the perforated faceplate. According to Maa's theory, the resistance and reactance of a MPP are given as:

$$\begin{aligned} Z_{resist} &= \frac{32\eta h_1}{d^2}\left(\sqrt{1+\frac{X^2}{32}} + \frac{\sqrt{2}dX}{32h_1}\right) \\ Z_{react} &= -i\rho_0\omega h_1\left(1 + \frac{1}{\sqrt{9+X^2/2}} + \frac{0.85d}{h_1}\right) \end{aligned} \tag{11}$$

where $X = d/2\sqrt{\rho_0\omega/\eta}$.

Upon combing Eq. (6) with Eq. (10), the velocity $v_1(\mathbf{r})$ can be given as:

$$v_1(\mathbf{r}) = -j\omega\lambda w_p(\mathbf{r}) + \gamma(p_1(\mathbf{r}) - p_2(\mathbf{r},h_1)) \tag{12}$$

where $\lambda = 1 - \sigma(Z_{react}/Z_0)$, $\gamma = \sigma/Z_0$ and $Z_0 = Z_{resist} + Z_{react}$.

Next, the fluid velocity adjacent to the lower face plate can be given as:

$$v_3(\mathbf{r}) = v_2(\mathbf{r},h_1+H) = -j\omega w_b(\mathbf{r}) \tag{13}$$

Substitution of Eqs. (3) and (2) into Eqs. (12) and (13) leads to:

$$\begin{aligned} v_2(\mathbf{r},h_1) &= (C-D)/\rho_0 c_0 = \\ &-j\omega\lambda w_p(\mathbf{r}) + \gamma(p_1(\mathbf{r}) - (C+D)) \end{aligned} \tag{14}$$

$$v_2(\mathbf{r},h_1+H) = \left(Ce^{jk_0H} - De^{-jk_0H}\right)/\rho_0 c_0 = -j\omega w_b(\mathbf{r}) \tag{15}$$

Combing Eqs. (14) and (15), one can express the unknown parameters C and D as:

$$\begin{aligned} D &= \rho_0 c_0\left[(1+\gamma\rho_0 c_0)e^{-jk_0H}j\omega w_b(\mathbf{r}) - j\omega\lambda w_p(\mathbf{r}) + \gamma p_1(\mathbf{r})\right]/Q \\ C &= \rho_0 c_0\left[-j\omega w_b(\mathbf{r})e^{-jk_0H}(-1+\gamma\rho_0 c_0) - j\omega\lambda w_p(\mathbf{r})e^{-2jk_0H} + \gamma p_1(\mathbf{r})e^{-2jk_0H}\right]/Q \end{aligned} \tag{16}$$

where $Q = (1+\gamma\rho_0 c_0)e^{-2jk_0H} - 1 + \gamma\rho_0 c_0$.

For the case that the two faceplates are connected (bonded) by the honeycomb core, the core is considered as rigid, and the displacements of the faceplates are regarded as consistent [40], namely:

$$w_p(\mathbf{r}) = w_b(\mathbf{r}) \tag{17}$$

where the subscripts "p" and "b" denote the perforated faceplate and the bottom faceplate without perforation, respectively. The displacements of the two faceplates are governed by:

$$\left(D_{p,b}\nabla^4 - m_{p,b}\omega^2\right)w(\mathbf{r}) = \Delta p_{p,b}(\mathbf{r}) \tag{18}$$

where $m_{p,b}$ are the surface densities of the faceplates, $D_{p,b}$ denote flexural rigidities, and $\Delta p_{p,b}(\mathbf{r})$ are the pressure differences.

The total pressure acting on the two faceplates can be given as:

$$\begin{aligned} \Delta p_p(\mathbf{r}) &= p_1(\mathbf{r}) - p_2(\mathbf{r},h_1) - I(\mathbf{r}) \\ \Delta p_b(\mathbf{r}) &= p_2(\mathbf{r},h_1+H) - p_3(\mathbf{r}) + I(\mathbf{r}) \end{aligned} \tag{19}$$

where $I(\mathbf{r})$ is the force exerted by the honeycomb core.

Substituting Eq. (16) into Eq. (19) yields:

$$\begin{aligned}\Delta p_p(\mathbf{r}) &= (1-Q_3)p_1(\mathbf{r}) - Q_1 w_b(\mathbf{r}) - Q_2 w_p(\mathbf{r}) - I(\mathbf{r})\\ \Delta p_b(\mathbf{r}) &= G_1 w_b(\mathbf{r}) + G_2 w_p(\mathbf{r}) + G_3 p_1(\mathbf{r}) - p_3(\mathbf{r}) + I(\mathbf{r})\end{aligned} \tag{20}$$

where

$$\begin{aligned}&Q_1 = 2e^{-jk_0 H} j\omega\rho_0 c_0/Q, Q_2 = \left[-j\omega\lambda(e^{-2jk_0 H}+1)\rho_0 c_0\right]/Q,\\ &Q_3 = \gamma(e^{-2jk_0 H}+1)\rho_0 c_0/Q\\ &G_1 = \left(1-\gamma\rho_0 c_0 + (1+\gamma\rho_0 c_0)e^{-2jk_0 H}\right)j\omega\rho_0 c_0/Q,\\ &G_2 = -2j\omega\lambda\rho_0 c_0 e^{-jk_0 H}/Q, G_3 = 2\gamma e^{-jk_0 H}\rho_0 c_0/Q\end{aligned} \tag{21}$$

Assuming $u_{p,b}(\mathbf{r})$ are the displacements of the two faceplates when they are excited by an unit force $\delta(\mathbf{r})$, one has:

$$\left(D_{p,b}\nabla^4 - m_{p,b}\omega^2\right)u_{p,b}(\mathbf{r}) = \delta(\mathbf{r}) \tag{22}$$

According to the definition of the convolution integral, the displacements of the faceplates can be expressed as:

$$w_{p,b}(\mathbf{r}) = \int_{-\infty}^{\infty} \Delta p_{p,b}(\mathbf{f}) \times u_{p,b}(\mathbf{r}-\mathbf{f})d\mathbf{f} \tag{23}$$

Substituting Eqs. (20) and (21) into Eq. (23), one can write these displacements as:

$$\begin{aligned}w_p(\mathbf{r}) &= \int_{-\infty}^{\infty}\left((1-Q_3)p_1(\xi) - Q_1 w_b(\xi) - Q_2 w_p(\xi) - I(\xi)\right)\times u_p(\mathbf{r}-\xi)d\xi\\ w_b(\mathbf{r}) &= \int_{-\infty}^{\infty}\left(G_1 w_b(\xi) + G_2 w_p(\xi) + G_3 p_1(\xi) - p_3(\xi) + I(\xi)\right)\times u_b(\mathbf{r}-\xi)d\xi\end{aligned} \tag{24}$$

The force of the honeycomb can be obtained by introducing the Fourier transform to Eq. (24) as well as by combing with the convolution theorem,

$$\begin{aligned}W_p(\mathbf{k}) &= 2\pi\left((1-Q_3)P_1(\mathbf{k}) - Q_1 W_b(\mathbf{k}) - Q_2 W_p(\mathbf{k}) - I_p(\mathbf{k})\right)U_p(\mathbf{k})\\ W_b(\mathbf{k}) &= 2\pi\left(G_1 W_b(\mathbf{k}) + G_2 W_p(\mathbf{k}) + G_3 P_1(\mathbf{k}) - P_3(\mathbf{k}) + I_p(\mathbf{k})\right)U_b(\mathbf{k})\end{aligned} \tag{25}$$

where $\mathbf{k} = (k_x, k_y)$ and $U_{p,b}(\mathbf{k}) = 1/2\pi\left(D_{p,b}|\mathbf{k}|^4 - m_{p,b}\omega^2\right)$. $W_{p,b}(\mathbf{k}), P_1(\mathbf{k})$, $I_p(\mathbf{k})$and $U_p(\mathbf{k})$ are the Fourier transforms of $w_{p,b}(\mathbf{r}), p_1(\mathbf{r}), I(\mathbf{r})$ and $u_{p,b}(\mathbf{r})$, which can be obtained by:

$$\begin{aligned}F(\mathbf{k}) &= \tfrac{1}{2\pi}\int_{-\infty}^{\infty} f(\mathbf{r})e^{-j\mathbf{kr}}d\mathbf{r}\\ f(\mathbf{r}) &= \int_{-\infty}^{\infty} F(\mathbf{k})e^{j\mathbf{kr}}d\mathbf{k}\end{aligned} \tag{26}$$

Substitution of Eq. (12) into Eq. (4) yields:

$$\begin{aligned}p_1(\mathbf{r}) = 2p_i(\mathbf{r},0) &- \frac{\rho_0\omega}{2}\\ &\times\int_{-\infty}^{\infty}\mathbf{H}_0^{(1)}(k_0|\mathbf{r}-\mathbf{r}_0|)\left(-j\omega\lambda w_p(\mathbf{r}) + \gamma(p_1(\mathbf{r}) - p_2(\mathbf{r},h_1))\right)d\mathbf{r}_0\end{aligned} \tag{27}$$

Since the function $\mathbf{H}_0^{(1)}(k_0|\mathbf{r}-\mathbf{r}_0|)$ is given as:

$$\mathbf{H}_0^{(1)}(k_0|\mathbf{r}-\mathbf{r}_0|) = \frac{1}{\pi}\int_{-\infty}^{\infty}\frac{e^{j\mathbf{k}(\mathbf{r}-\mathbf{r}_0)}}{\sqrt{k_0^2 - |\mathbf{k}|^2}}d\mathbf{k} \tag{28}$$

Eq. (27) can be rewritten after the Fourier transform, as:

$$P_1(\mathbf{k}) = \frac{2}{Q_p}\delta(\mathbf{k}) - \frac{Q_w}{Q_p}W_b(\mathbf{k}) \tag{29}$$

where

$Q_p = \left(1+\rho_0\omega\gamma(e^{-2jk_0 H}-1)/Q\sqrt{k_0^2-|\mathbf{k}|^2}\right)$, $Q_w = \rho_0\omega(-2\gamma\rho_0 c_0 e^{-jk_0 H}j\omega - j\omega\lambda(e^{-2jk_0 H}-1))/Q\sqrt{k_0^2-|\mathbf{k}|^2}$.

Similarly, by applying Fourier transform to Eq. (5), one arrives at:

$$P_3(\mathbf{k}) = Q_{p3}W_b(\mathbf{k}) \tag{30}$$

where $Q_{p3} = -j\rho_0\omega^2/\sqrt{k_0^2-|\mathbf{k}|^2}$.

Substituting Eqs. (29) and (30) into Eq. (25), one obtains the displacement as:

$$W_b(\mathbf{k}) = F_b(\mathbf{k})\delta(\mathbf{k}) \tag{31}$$

where $F_b(\mathbf{k}) = 2(G_3 - Q_3 + 1)/Q_p Q_L$, $Q_L = Q_{wm} + (G_3 - Q_3 + 1)Q_w/Q_p + Q_{p3}$ and $Q_{wm} = (D_p + D_b)|\mathbf{k}|^4 - \Gamma\omega^2 + j\omega\rho_0 c_0/Q\left[-(1-e^{-jk_0 H})^2(1+\lambda) + \gamma\rho_0 c_0(1-e^{-2jk_0 H})\right]$, Γ is the sum of surface densities of the two face plates, given as $\Gamma = m_p + m_b$.

Given that the two faceplates are connected by the honeycomb core, the mass of the honeycomb should be reflected in the model. The total surface density Γ is thus modified by adding the surface density of the honeycomb core m_c,

$$\Gamma^c = \Gamma + m_c \tag{32}$$

where the surface densities of the honeycomb cores are calculated by

$$m_c = \frac{M}{S} = \begin{cases}\left(1.5\sqrt{3}a^2 - 1.5\sqrt{3}\left(a - t/\sqrt{3}\right)^2\right)H\rho_c/1.5\sqrt{3}a^2 & \text{Hexgonal core}\\ (a_r b_r - (a_r - t_r)(b_r - t_r))H\rho_c/a_r b_r & \text{Rectangular core}\\ \left(a_t^2 - \left(a_t - \sqrt{3}t_t\right)^2\right)H\rho_c/a_t^2 & \text{Triangualr core}\end{cases} \tag{33}$$

where M and S are the unit cell mass and cross section area of the honeycomb cores respectively, ρ_c is the density of the honeycomb cores.

Substitution of Eq. (31) into Eq. (26) yields the displacement of the bottom facelate:

$$w_b(\mathbf{r}) = \frac{2(G_3 - Q_3 + 1)}{Q_{b1} + Q_{b2} + Q_{b2}} \tag{34}$$

where Q_{b1}, Q_{b2} and Q_{b3} are:

$$\begin{aligned}&Q_{b1} = (1+\rho_0\omega\gamma(e^{-2jk_0 H}-1)/Qk_0)\\ &\left(-\Gamma^c\omega^2 + j\omega\rho_0 c_0/Q\left[-(1-e^{-jk_0 H})^2(1+\lambda) + \gamma\rho_0 c_0(1-e^{-2jk_0 H})\right]\right)\\ &Q_{b2} = (G_3 - Q_3 + 1)(-G_3\rho_0 c_0 j\omega + Q_2 + 2\rho_0 c_0 j\omega\lambda/Q)\\ &Q_{b3} = -j\rho_0 c_0\omega(G_1/j\omega\rho_0 c_0 + Q_3 - 2/Q)\end{aligned} \tag{35}$$

Similarly, Substitution of Eq. (29) into Eq. (26) leads to the pressure on the surface of the top faceplate:

$$p_1(\mathbf{r}) = \frac{2j\omega\rho_0 c_0 Q}{QG_1 + j\omega\rho_0 c_0 QQ_3 - 2j\omega\rho_0 c_0}\left(1 - \frac{(G_3 - Q_3 + 1)Q_m}{Q(Q_{b1} + Q_{b2} + Q_{b2})}\right) \tag{36}$$

where $Q_m = -G_3\rho_0 c_0 j\omega Q + Q_2 Q + 2\rho_0 c_0 j\omega\lambda$.

Combing Eqs. (6), (14), (16), (17), (34) and (36) yields

$$v_1(\mathbf{r}) = (Q_{v1}/Q)w_b(\mathbf{r}) + (Q_{v2}/Q)p_1(\mathbf{r}) \tag{37}$$

where $Q_{v2} = \gamma(e^{-2jk_0 h} - 1)$ and $Q_{v1} = -2\gamma\rho_0 c_0 e^{-jk_0 h}j\omega - j\omega\lambda(e^{-2jk_0 h} - 1)$.

According to Eq. (32), the sound pressure and velocity in the transmitted sound field are:

$$\begin{aligned}p_3(\mathbf{r}) &= -i\rho_0 c_0\omega w_b(\mathbf{r})\\ v_3(\mathbf{r}) &= -i\omega w_b(\mathbf{r})\end{aligned} \tag{38}$$

Finally, the STL and SAC of the honeycomb sandwich with perforated faceplate can be obtained by comparing the transmitted and reflected sound energy with the incident energy, as:

$$STL = 20\log_{10}\frac{I_i}{I_t}\ SAC = 1 - \frac{I_r}{I_i} - \frac{I_t}{I_i} \tag{39}$$

here, I_i, I_t and I_r are the total incident energy, the transmitted energy and the reflected energy, respectively, which can be calculated as:

$$\begin{aligned} I_i &= 0.5\mathrm{Re}\int_S p_i(\mathbf{r})\cdot v_i^*(\mathbf{r})dS \\ I_t &= 0.5\mathrm{Re}\int_S \{p_3(\mathbf{r})\cdot v_3^*(\mathbf{r})\}dS \\ I_r &= 0.5\mathrm{Re}\int_S \{(p_1(\mathbf{r})-p_i(\mathbf{r}))\cdot(-v_1(\mathbf{r})+v_i(\mathbf{r}))^*\}dS \end{aligned} \tag{40}$$

4. Validation

The proposed theory in the last section should be validated because of the simplifications and assumptions made to develop the model. To this end, a FE model is established based on the commercial software COMSOL Multiphysics. The calculation unit cells of sandwich panels with perforated facing are shown in Fig. 3 for hexagonal core, rectangular core and triangular core. The shapes of these unit cells are all rectangular, so that periodic boundary conditions can be added to the boundary of each unit cell. The calculation model of hexagonal sandwich panel is shown in Fig. 4, where two perfectly matched layers are added to the ends of incident and transmitted sound fields to mimic open and non-reflecting infinite sound fields. The solid mechanics modulus of COMSOL is applied to calculate the displacement and velocity of the solid part of each sandwich panel, with the sandwich regarded as an isotropic elastic material. For air inside the perforated pore, the thicknesses of viscous and thermal boundary layers have the same order of magnitude as the pore radius in the considered frequency range. Therefore, the thermoacoustic modulus is applied to calculate the sound pressure and temperature variation of the air, with both viscous and thermal losses included. With air in the incident, transmitted and inside the core considered as non-viscous, the pressure acoustic modulus is applied to calculate the pressure and air velocity. At solid-fluid interface, the velocity of air is equal to that of solid, and temperature variation is adiabatic at the interface.

The FE simulation results of honeycomb sandwich panels with perforated facings are compared with theoretical model predictions in Fig. 5 from the viewpoint of STL and SAC, respectively. All the samples are assumed to be made of aluminum with density of 2700 kg/m^3, Poisson's ratio of 0.35, and elastic modulus of 70 GPa. The geometrical parameters of the samples are listed in Table 1. The simulated results for sandwich panels with hexagonal, rectangular and triangular cores all agree well with theoretical predictions.

Except from the simulation results by FE models, the present theory is also validated by comparison with the available results in literature. The solid frames of the perforated honeycomb sandwich panels can be favorably degraded to rigid by setting the flexural rigidity and surface density of the faceplates to very large values (e.g. $D_{p,b} = 10^{10}\mathrm{Pa}\cdot\mathrm{m}^3$, $m_{p,b} = 10^5\mathrm{kg/m}^2$). The sound absorption coefficient of the rigid perforated sandwich panel is then compared with that derived by Tang et al.'s theory [37] which

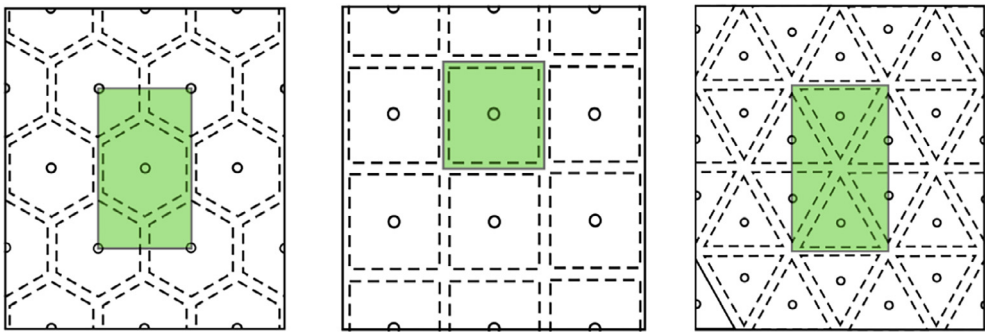

Fig. 3. Unit cells of honeycomb sandwich panels with perforated faceplates for FE simulation.

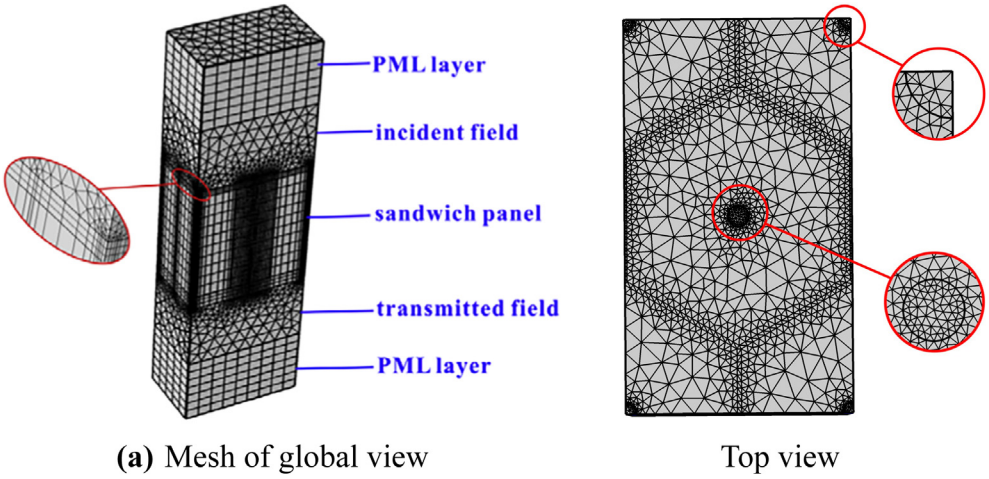

Fig. 4. FE mesh of perforated hexagonal honeycomb sandwich panel.

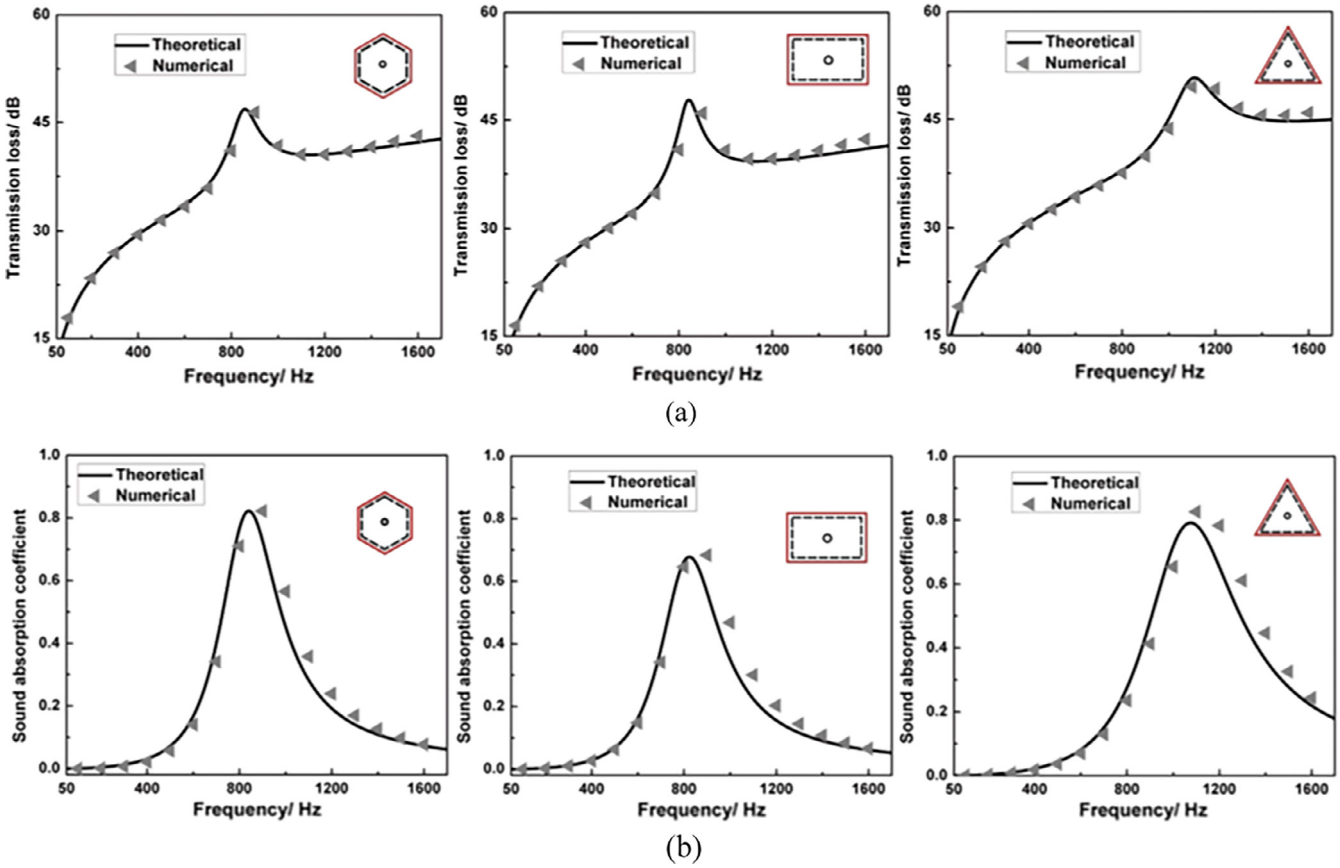

Fig. 5. Comparison of STL (a) and SAC (b) between theory and FE simulation for sandwich panel with various honeycomb cores.

calculates the sound absorption of rigid frame microperforated sandwich panels as shown in Fig. 6. The geometrical parameters of the rigid microperforated sandwich panel with rectangular core are the same as that listed in Table 1. It is clear that the present theory agrees well with Tang et al.'s theory for the sound absorption prediction.

In addition, since the honeycomb sandwich panel with perforated face plate can be degraded to non-perforated classic honeycomb sandwich panel when the perforation ratio and perforated pore diameter are negligibly small, the present theory is therefore verified by Kumar et al.'s [24] model for classical honeycomb sandwich panels as shown in Fig. 7. Kumar et al. calculated the STL of classical honeycomb sandwich panels by orthotropic panel theory. The geometrical parameters of the non-perforated hexagonal honeycomb sandwich panel in Fig. 7 are the same as that listed in Table 1 except from the perforation ratio and pore diameter. It can be seen from Fig. 7 that STL by the present theory agrees well with that by Kumar et al.'s model.

Table 1
Geometrical parameters of perforated honeycomb sandwich panels for FE simulation.

Hexagonal core
$h_1 = 1$ mm, $h_1 = 2$ mm, H = 17 mm, a = 6.2 mm, t = 0.2 mm, d = 1 mm,$\sigma = 0.79\%$
Rectangular core
$h_1 = 1$ mm, $h_1 = 1$ mm, H = 20 mm, $a_r = 12$ mm, $b_r = 10$ mm, t = 0.3 mm, d = 1.2 mm,$\sigma = 0.94\%$
Triangular core
$h_1 = 1$ mm, $h_1 = 2$ mm, H = 17 mm, $a_t = 10$ mm, t = 0.2 mm, d = 0.8 mm,$\sigma = 1.16\%$

5. Parameter study

To figure out the effects of perforated faceplate and explore the influential parameters related to the perforation, systematic parameter studies based on the validated analytical model are performed from the viewpoint of STL and SAC. For further validation of the model, corresponding results obtained using FE models are also presented below.

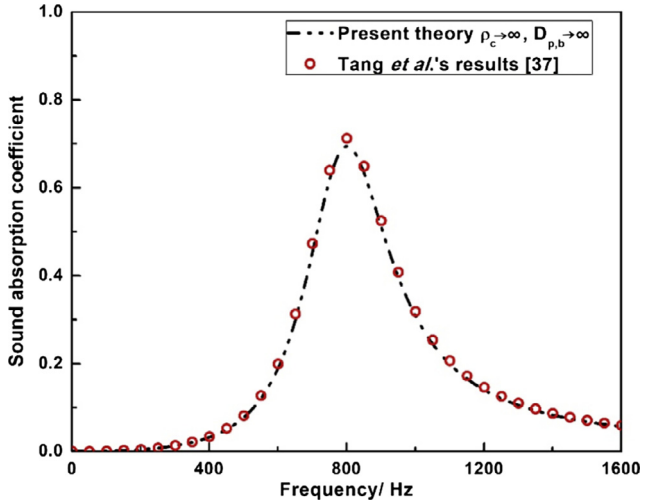

Fig. 6. Comparison of SAC between the present model and results by Tang et al. [37].

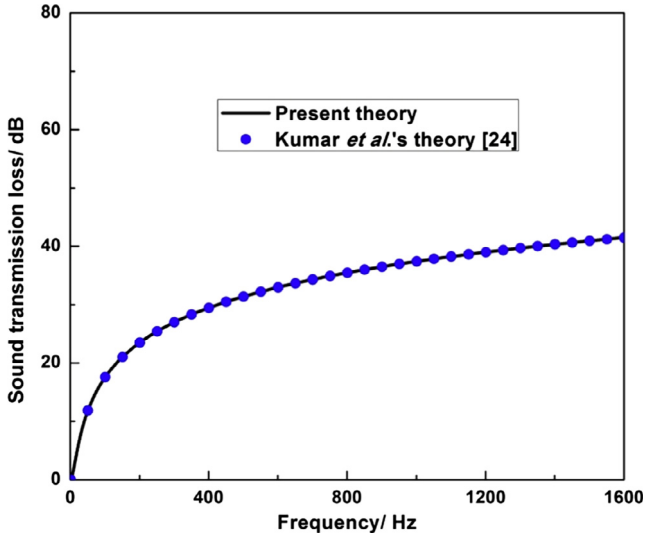

Fig. 7. Comparison of STL between the present model and results by Kumar et al. [24].

5.1. Effect of perforated faceplate

The STL and SAC of hexagonal sandwich panels with perforated faceplates are compared with those of hexagonal sandwich panel without perforation in Fig. 8. Geometrical parameters of the sandwich are the same as those listed in Table 1.

It can be seen from Fig. 8(b) that, in the absence of perforation, the SAC is zero for all frequencies as expected. That is, traditional honeycomb sandwiches without perforated facings cannot absorb sound at all. In sharp contrast, for sandwiches with perforated faceplates, an absorption crest appears in the SAC versus frequency curve, because the perforated faceplate, the honeycomb core and the backing faceplate constitute distributed Helmholtz resonators. The resonance frequency of the distributed 'Helmholtz resonators' can be estimated as [44]

$$f_0 = \frac{c_0}{2\pi}\sqrt{\sigma/H(h_1+\delta_{tot})} \approx 860\text{Hz} \tag{41}$$

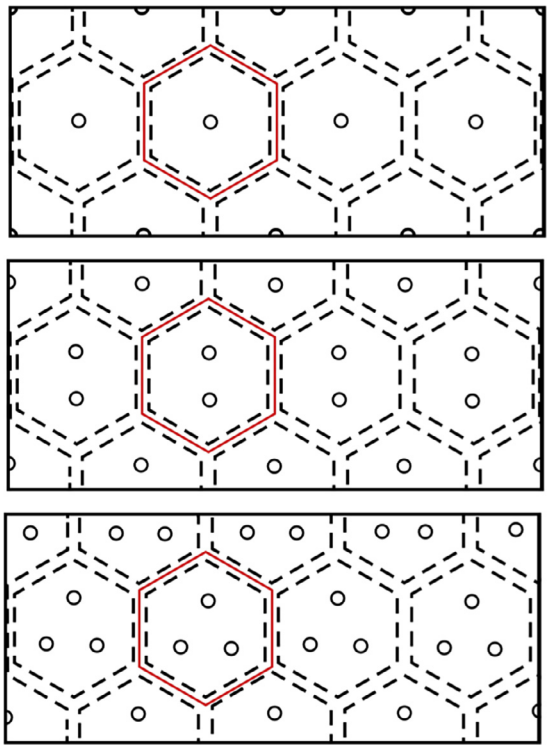

Fig. 9. Schematic of hexagonal sandwich panels with different perforation ratios.

where $\delta_{tot} \approx 8d/3\pi$ is the end correction. The results of Fig. 8(b) demonstrate that the peak frequency in the SAC curve as predicted by the present analytical model is approximately equal to the resonance frequency estimated by Eq. (41).

Fig. 8(a) shows perforation-induced increment of STL within the frequency range of 700–1200 Hz. The peak frequency in the STL curve is identical to that in the SAC curve, which means that the enlargement of STL should be attributed to the appearance of SAC. For the sandwich without perforation, since no acoustic energy can be consumed during sound propagation, the STL is decided by the reflection of sound wave. In the presence of perforation, sound wave enters the sandwich via the perforated pores

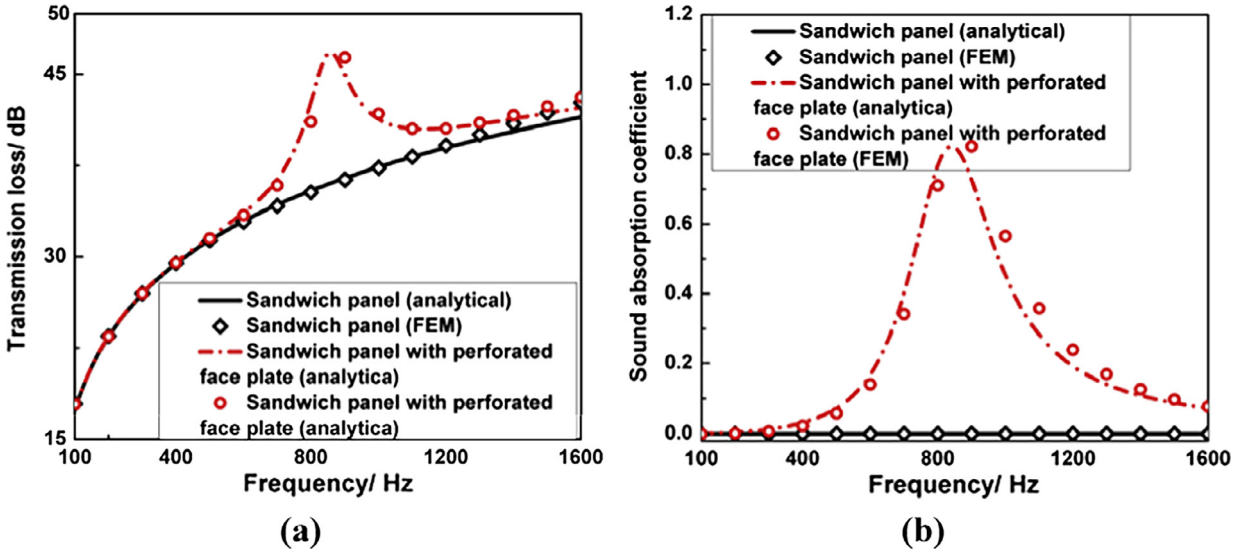

Fig. 8. Comparison of sound transmission loss and absorption coefficient between sandwich panels with non-perforated and perforated faceplates.

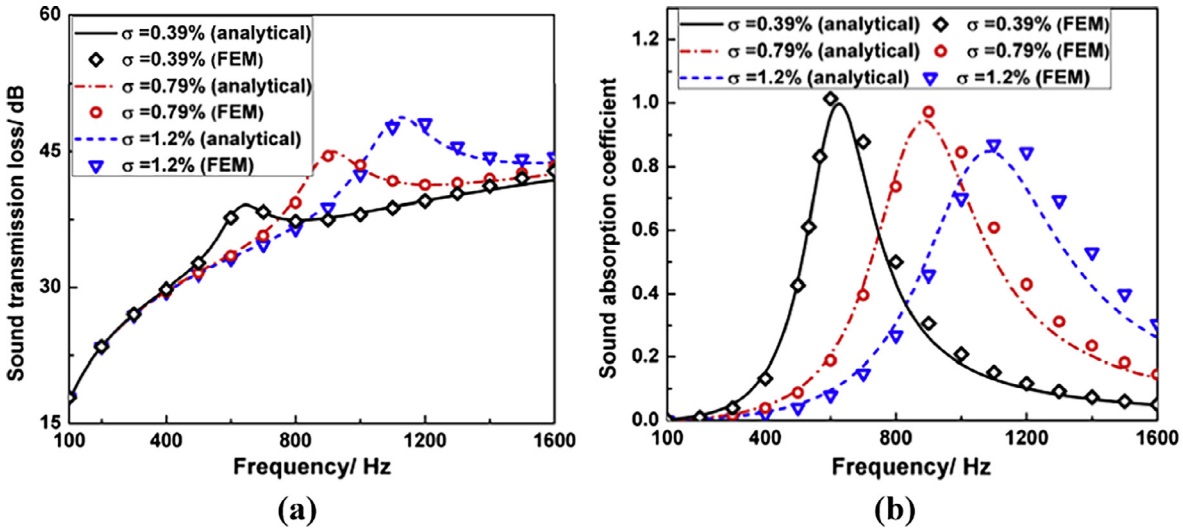

Fig. 10. Influence of perforation ratio on sound transmission loss and absorption coefficient of hexagonal sandwich panel.

and the acoustic energy is consumed due to viscous and thermal losses inside the pores.

5.2. Influence of perforation ratio

Fig. 9 shows three hexagonal sandwich panels having identical geometrical parameters but different perforation ratios. These sandwich panels have one, two and three pores in each unit cell of the faceplate as shown in Fig. 9. All the pores have the same diameter of 0.5 mm, and the other geometrical parameters of the sandwich panels are the identical to those of Table 1. Accordingly, the perforation ratios are 0.39%, 0.79% and 1.2%, respectively.

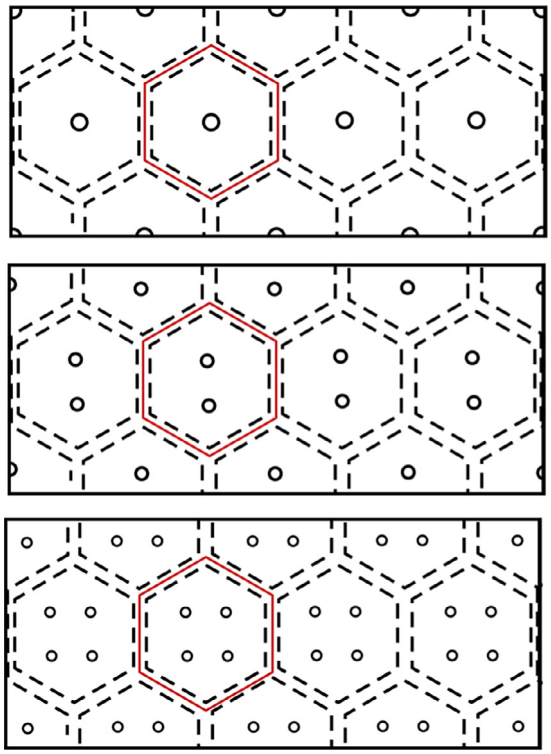

Fig. 11. Schematic of hexagonal sandwich panels with different pore diameters but fixed perforation ratio.

The influence of perforation ratio on the STL and SAC of hexagonal sandwich panels is displayed in Fig. 10. It can be seen from Fig. 10 that with the increase of perforation ratio, the peak frequency of the STL and SAC increases, which can also be seen evidently from Eq. (41). Besides, the bandwidth for SAC is enlarged by the increase of perforation ratio. As the perforation ratio is increased, the viscous and thermal losses inside the perforated pores are enhanced as a result of the increased contact area between air and solid frame, thus enlarging the resistance of the perforated faceplate. The enlarged resistance will increase the bandwidth [45].

5.3. Influence of pore diameter

Fig. 11 shows three hexagonal sandwich panels having the same geometrical parameters except the pore diameter and number. These sandwich panels have one, two and four pores in each unit cell of the top faceplate. With identical perforation ratio assumed, the corresponding pore diameters are 1 mm, 0.707 mm and 0.5 mm. The remaining parameters are the same as those listed in Table 1.

Fig. 12 compares the STL and SAC of the three sandwich panels. It is seen from Fig. 12 that the peak frequency is improved by reducing the pore diameter. According to Eq. (41), the peak frequency of SAC increases with decreasing pore diameter and, accordingly, the peak frequency of STL increases. Besides, with the decrease of pore diameter, the bandwidth of SAC is enlarged. Decreasing the pore diameter increases the contact area between air and solid frame inside the pores, which in turn leads to enlarged resistance of the perforated faceplate.

5.4. Influence of core configuration

According to the theory presented in Section 3, the surface density and perforation ratio of a honeycomb sandwich panel are affected by core configuration. Consequently, the STL and SAC of the sandwich are also affected, as discussed below.

Let sandwich panels with different honeycomb cores have the same geometrical parameters and the same effective mass. When the geometrical parameters of hexagonal sandwich panel are the same as shown in Table 1, the side lengths of rectangular and triangular cores can be calculated using Eq. (21). Table 2 presents the side length and perforation ratio for each type of sandwich

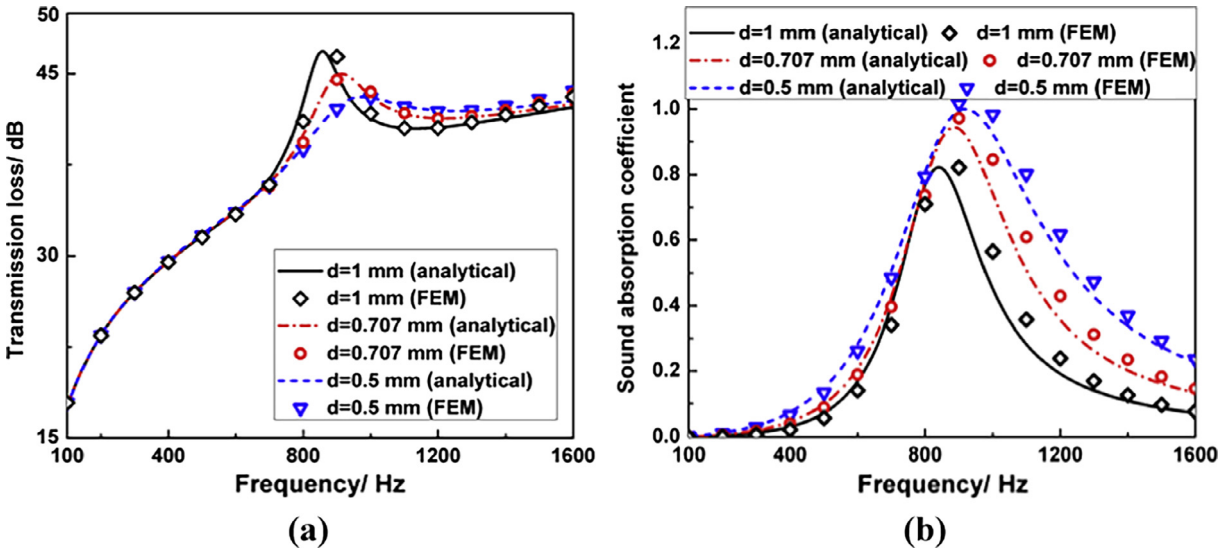

Fig. 12. Influence of pore diameter on sound transmission loss and absorption coefficient of hexagonal sandwich panels with fixed perforation ratio.

Table 2
Side lengths of honeycomb cores and perforation ratios of sandwich panels with these cores.

Core shape	Side length (mm)	Perforation ratio
Hexagon	6.2	0.79%
Square	10.75	0.68%
Triangular	18.61157	0.52%

panel. For simplification, the length of the rectangular core is set as $a_s = b_s$.

The STL and SAC of the three sandwich panels are compared in Fig. 13. It is seen that the peak frequency increases as the edge number of the core is increased, and sandwich panel with triangular core has the best acoustic properties at relatively low frequencies.

6. Conclusion

An analytical model for estimating the STL and SAC of honeycomb sandwich panels with perforated faceplates is developed by taking into account the effect of faceplate perforation as well as the effect of core configuration. The reflected and transmitted sound pressures are expressed by applying the Green's function and solved by employing Fourier transforms. The STL and SAC are obtained by comparing the reflected and transmitted sound energy with the incident sound energy. FE models are developed to validate the analytical model, with good agreement achieved. In the analytical model, the two face plates are assumed to have the same displacement because of the honeycomb connection, which makes the presented model valid for frequencies lower than faceplate resonance frequency. Acoustic properties of frequencies higher than the faceplate resonance frequency go beyond our investigation in the present model but are part of our following research project. Influences of faceplate perforation, perforation ratio, pore size, and core configuration are discussed using the analytical model. Results show that perforation in faceplate can improve the STL and SAC at low frequencies, and the peak frequency in the STL and SAC curves increases with increasing perforation ratio and decreasing pore size. Compared with other sandwich panels of the same effective mass and perforated pores, the sandwich panel with triangular core exhibits the lowest peak

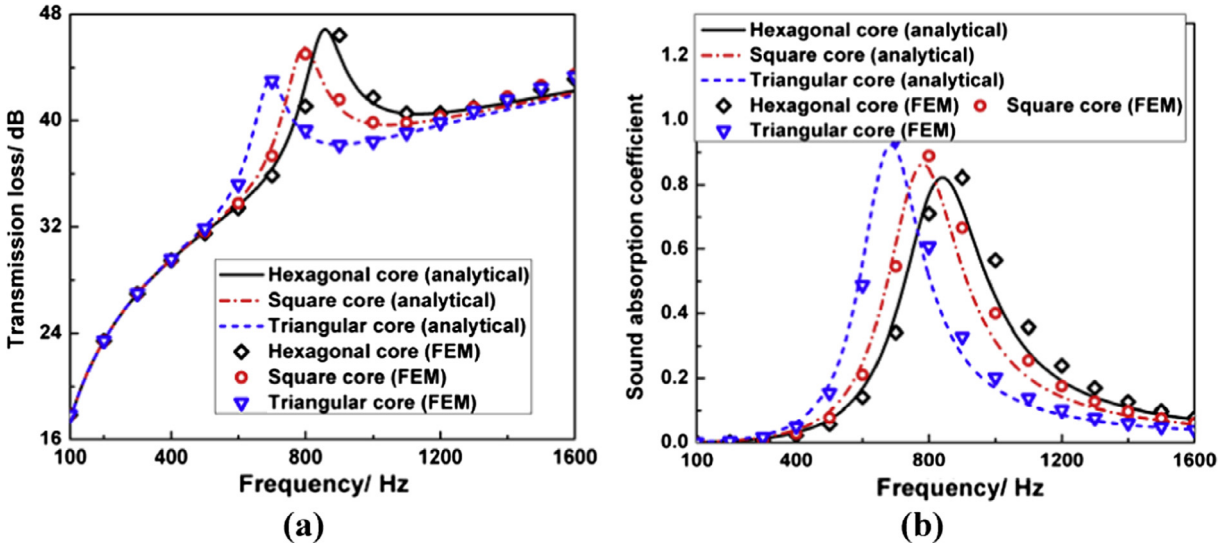

Fig. 13. Influence of core configuration on sound transmission loss and absorption coefficient of honeycomb sandwich panels having identical effective mass.

frequency for both STL and SAC. Results of the presented paper can inspire researchers to design multifunctional lightweight sandwich structures with superior mechanical and acoustic properties by artificially adding perforations to existing sandwich panels or optimizing the sandwich core.

Acknowledgements

H. Meng was sponsored by China Scholarship Council as a joined Ph. D. student in Ecole Centrale de Lyon. This work was supported by the National Natural Science Foundation of China (51528501 and 11532009) and the Fundamental Research Funds for Central Universities (2014qngz12). This work was performed within the framework of the Labex CeLyA of Universite de Lyon, the program Investissements d'Avenir (ANR-10-LABX-0060/ ANR-11-IDEX-0007) operated by the French National Research Agency (ANR).

References

[1] London A. Transmission of reverberant sound through double walls. J. Acoust. Soc. Am. 1950;22:270–9.
[2] António J, Tadeu A, Godinho L. Analytical evaluation of the acoustic insulation provided by double infinite walls. J. Sound. Vib. 2003;263:113–29.
[3] Chazot JD, Guyader JL. Prediction of transmission loss of double panels with a patch-mobility method. J. Acoust. Soc. Am. 2007;121:267–78.
[4] Wang T, Li S, Rajaram S, Nutt SR. Predicting the sound transmission loss of sandwich panels by statistical energy analysis approach. J. Vib. Acoust. 2010;132. 011004-7.
[5] Bolton JS, Green E. Normal incidence sound transmission through double-panel systems lined with relatively stiff, partially reticulated polyurethane foam. Appl. Acoust. 1993;39:23–51.
[6] Bolton JS, Shiau NM, Kang YJ. Sound transmission through multi-panel structures lined with elastic porous materials. J. Sound. Vib. 1996;191 (3):317–47.
[7] Panneton R, Atalla N. Numerical prediction of sound transmission through finite multilayer systems with poroelastic materials. J. Acoust. Soc. Am. 1996;100:346–54.
[8] Kang YJ, Bolton JS. A finite element model for sound transmission through foam-lined double-panel structures. J. Acoust. Soc. Am. 1996;99:2755–65.
[9] Biot MA. Theory of propagation of elastic waves in a fluid-saturated porous solid. I. Low-frequency range. J. Acoust. Soc. Am. 1956;28:168–78.
[10] Biot MA. Theory of propagation of elastic waves in a fluid-saturated porous solid. II. Higher frequency range. J. Acoust. Soc. Am. 1956;28:179–91.
[11] Chazot JD, Guyader JL. Transmission loss of double panels filled with porogranular materials. J. Acoust. Soc. Am. 2009;126:3040–8.
[12] Doutres O, Atalla N. Acoustic contributions of a sound absorbing blanket placed in a double panel structure: absorption versus transmission. J. Acoust. Soc. Am. 2010;128(2):664–71.
[13] Ghanbari M, Hossainpour S, Rezazadeh G. Studying thin film damping in a micro-beam resonator based on non-classical theories. Acta Mech Sinica 2016;32:369–79.
[14] Zielinski TG, Galland M-A, Ichchou M. Fully coupled finite-element modeling of active sandwich panels with poroelastic core. J. Vib. Acoust. 2012;134:021007.
[15] Hu Y, Galland M-A, Chen K. Acoustic transmission performance of double-wall active sound packages in a tube: numerical/experimental validations. Appl. Acoust. 2012;73:323–37.
[16] Melon M, Herzog P, Sitel A, Galland M-A. One dimensional study of a module for active/passive control of both absorption and transmission. Appl. Acoust. 2012;73:234–42.
[17] Shen C, Xin FX, Lu TJ. Theoretical model for sound transmission through finite sandwich structures with corrugated core. Int. J. Nonlin. Mech. 2012;47:1066–72.
[18] Sun W, Liu Y. Vibration analysis of hard-coated composite beam considering the strain dependent characteristic of coating material. Acta Mech. Sinica 2016;32:731–42.
[19] Mead DJ. Wave propagation in continuous periodic structures: research contributions from Southampton 1964–1995. J. Sound. Vib. 1996;190:495–524.
[20] Wang J, Lu TJ, Woodhouse J, Langley RS, Evans J. Sound transmission through lightweight double-leaf partitions: theoretical modelling. J. Sound. Vib. 2005;286:817–47.
[21] Craik RJM, Smith RS. Sound transmission through lightweight parallel plates. Part II: structure-borne sound. Appl. Acoust. 2000;61:247–69.
[22] Xin FX, Lu TJ. Sound radiation of orthogonally rib-stiffened sandwich structures with cavity absorption. Compos. Sci. Technol. 2010;70:2198–206.
[23] Shen C, Xin FX, Cheng L, Lu T. Sound radiation of orthogonally stiffened laminated composite plates under airborne and structure borne excitations. Compos. Sci. Technol. 2013;84:51–7.
[24] Kumar S, Feng L, Orrenius U. Predicting the sound transmission loss of honeycomb panels using the wave propagation approach. Acta. Acust. United. Ac 2011;97:869–76.
[25] Jung J-D, Hong S-Y, Song J-H, Kwon H-W. A study on transmission loss characteristics of honeycomb panel for offshore structures. J. Appl. Math. Phys. 2015;3:172.
[26] Huang WC, Ng CF. Sound insulation improvement using honeycomb sandwich panels. Appl. Acoust. 1998;53:163–77.
[27] Ng CF, Hui CK. Low frequency sound insulation using stiffness control with honeycomb panels. Appl. Acoust. 2008;69:293–301.
[28] Griese D, Summers JD, Thompson L. The effect of honeycomb core geometry on the sound transmission performance of sandwich panels. J. Vib. Acoust. 2015;137:021011.
[29] Feng L, Ramanathan SK. On application of radiation loss factor in the prediction of sound transmission loss of a honeycomb panel. Int. J. Acoust. Vib. 2012;17:47–51.
[30] Maa D-Y. Theory and design of microperforated panel sound-absorbing constructions. Sci. China 1975;18:38–50.
[31] Maa D-Y. Potential of microperforated panel absorber. J. Acoust. Soc. Am. 1998;104:2861–6.
[32] Atalla N, Sgard F. Modeling of perforated plates and screens using rigid frame porous models. J. Sound. Vib. 2007;303:195–208.
[33] Asdrubali F, Pispola G. Properties of transparent sound-absorbing panels for use in noise barriers. J. Acoust. Soc. Am. 2007;121:214–21.
[34] Li G, Mechefske CK. A comprehensive experimental study of micro-perforated panel acoustic absorbers in MRI scanners. Magn. Reson. Mater. Phys. 2010;23:177–85.
[35] Sakagami K, Morimoto M, Yairi M. Application of microperforated panel absorbers to room interior surfaces. Int. J. Acoust. Vib. 2008;13:120–4.
[36] Dupont T, Pavic G, Laulagnet B. Acoustic properties of lightweight micro-perforated plate systems. Acta Acust. United. Ac. 2003;89:201–12.
[37] Tang Y, Li F, Xin FX, Lu TJ. Heterogeneously perforated honeycomb-corrugation hybrid sandwich panel as sound absorber. Mater. Des. 2017;134:502–12.
[38] Bravo T, Maury C, Pinhède C. Sound absorption and transmission through flexible micro-perforated panels backed by an air layer and a thin plate. J. Acoust. Soc. Am. 2012;131:3853–63.
[39] Bravo T, Maury C, Pinhède C. Enhancing sound absorption and transmission through flexible multi-layer micro-perforated structures. J. Acoust. Soc. Am. 2013;134:3663–73.
[40] Toyoda M, Takahashi D. Sound transmission through a microperforated-panel structure with subdivided air cavities. J. Acoust. Soc. Am. 2008;124:3594–603.
[41] Takahashi D. Sound transmission through single plates with absorptive facings: improved theory and experiment. J. Acoust. Soc. Am. 1990;88:879–82.
[42] Toyoda M, Takahashi D. Reduction of acoustic radiation by impedance control with a perforated absorber system. J. Sound. Vib. 2005;286:601–14.
[43] Toyoda M, Tanaka M, Takahashi D. Reduction of acoustic radiation by perforated board and honeycomb layer systems. Appl. Acoust 2007;68:71–85.
[44] R.T. Randeberg, Perforated panel absorbers with viscous energy dissipation enhanced by orifice design, Doctoral Thesis, 2000, pp. 9.
[45] Maa D-Y. General theory and design of microperforated-panel absorbers. Acta Acust 1997;22:385–93.